2016 IEEE Intelligent Vehicles Symposium (IV)
Gothenburg, Sweden, June 19-22, 2016

A Direct Scattering Model for Tracking Vehicles with High-Resolution Radars

Christina Knill[1], Alexander Scheel[2], and Klaus Dietmayer[2]

Abstract— **In advanced driver assistance systems and autonomous driving, reliable environment perception and object tracking based on radar is fundamental. High-resolution radar sensors often provide multiple measurements per object. Since in this case traditional point tracking algorithms are not applicable any more, novel approaches for extended object tracking emerged in the last few years. However, they are primarily designed for lidar applications or omit the additional Doppler information of radars. Classical radar based tracking methods using the Doppler information are mostly designed for point tracking of parallel traffic. The measurement model presented in this paper is developed to track vehicles of approximately rectangular shape in arbitrary traffic scenarios including parallel and cross traffic. In addition to the kinematic state, it allows to determine and track the geometric state of the object. Using the Doppler information is an important component in the model. Furthermore, it neither requires measurement preprocessing, data clustering, nor explicit data association. For object tracking, a Rao-Blackwellized particle filter (RBPF) adapted to the measurement model is presented.**

I. Introduction

Precise, reliable and robust vehicle environment perception is an essential basis for today's and future advanced driver assistance systems and autonomous driving. Since radar sensors have the advantage to be able to accurately measure radial distances and furthermore relative velocities of other objects, they are already utilized in today's automotive safety and assistance systems such as adaptive cruise control (ACC) or parking aid systems. Moreover, compared to other automotive sensors, such as lidar or camera, they are more robust considering environmental influences such as weather or dirt. Novel high-resolution radar sensors often provide multiple measurements per object. Objects giving rise to multiple measurements at a sensor in a single time frame are referred to as extended objects. Since traditional point tracking algorithms are not applicable in these scenarios, new approaches to track extended objects are developed to benefit from the additional information of the measurements. Generally, they can be split in two groups: Algorithms based on traditional point tracking using data preprocessing and methods for extended object tracking.

Approaches using traditional point tracking methods require data preprocessing to reduce multiple measurements to a single object hypothesis. However, this step usually involves loss of information. In [1], [2], object state parameters such as its velocity, yaw rate or orientation are first estimated based on multiple high-resolution radar measurements of one or more sensors independently of the underlying point tracking algorithm. Since this approach depends on solving a system of equations that needs to be over-determined in order to obtain a reliable solution, a large number of measurements per frame is required. This is not always the case especially in the sensors' far field and crowded scenarios with occlusions. An approach for modeling and simulating radar measurements of vechicles is presented in [3]. It is proposed to partition a vehicle in reflection centers and the measurements are associated to those. Tracking implementations are presented in [4] and [5].

Examples for novel extended object tracking approaches are the spatial distribution model [6], [7], the random hypersurface model [8], [9], and the random matrix model [10]–[12]. However, none of these approaches is designed for radar applications. Furthermore, the random hypersurface as well as the spatial distribution model approaches both rely on a feasible model of a known spatial distribution of measurements on the target. Also, in many cases the measurement likelihood convolution integral is hard to solve. The random matrix model assumes an elliptic object shape which is not a suitable representation for vehicles which exhibit an approximately rectangular shape in 2D data. Moreover, the valuable Doppler velocity cannot be utilized in this approach. Another interesting extended object method for tracking vehicles in lidar data has been presented by Petrovskaya and Thrun [13]. It uses a rectangular representation for the vehicle's shape and evaluates the measurement likelihood by intersecting the rectangles with the individual laser rays. In a sense, this method uses a direct scattering approach in that it computes expected measurements for given object states and then compares them to the obtained measurements. This is contrary to many preprocessing routines which try to determine the object state from received measurements and thus try to solve the inverse and often more difficult problem.

In this paper, the idea of using a direct scattering approach is seized and transferred to tracking with high-resolution radars. A measurement model for high-resolution radar is presented, which allows to describe and determine the state and extent of an extended object in every sensor-to-object alignment. For radar applications, dealing with longitudinal velocities is a rather trivial task since the Doppler velocity is approximately identical to the vehicle motion. Dealing with arbitrary motion and cross traffic is far more complex due to nonlinear relations between object motion and Doppler velocity. Additionally, ambiguities considering the direction

[1] C. Knill is with Institute of Microwave Engineering, Ulm University, 89081 Ulm, Germany christina.knill@uni-ulm.de

[2] A. Scheel and K. Dietmayer are with Institute of Measurement, Control & Microtechnology, Ulm University, 89081 Ulm, Germany alexander.scheel@uni-ulm.de, klaus.dietmayer@uni-ulm.de

of motion have to be handled. Furthermore, the model should be independent of the number of available measurements and robust in the presence of clutter. The measurement model presented in the following is designed to incorporate these properties. Furthermore, it is deployed in a Rao-Blackwellized particle filter (RBPF) to track single vehicles using data of a single sensor.

In the next Section, the state and measurement vectors are introduced. The new measurement model is presented in Section III and its Rao-Blackwellized particle filter implementation is outlined in Section IV. Experimental results of the filter on real radar data are presented in Section V.

II. State and Measurement Representation

Two different coordinate systems and representations are required in this approach for vehicle environment perception. The first is the polar sensor coordinate (SC) system. Its origin is located at the sensor mount point on the vehicle and the 0°-axis is aligned with the sensor's boresight. The second is the Cartesian vehicle coordinate (VC) system. Its origin is equal to the center of motion of the ego-vehicle. The x-axis is aligned with the vehicles direction of motion and the y-axis is pointing to its left side.

A. State Vector

The state vector $\boldsymbol{\xi}_k = \begin{bmatrix}\boldsymbol{x}_k, & \boldsymbol{g}_k\end{bmatrix}^\mathrm{T}$ of an object at time index k is split up into a kinematic part $\boldsymbol{x}_k$ and a geometric part $\boldsymbol{g}_k$. The kinematic part includes the object's center of motion defined as the center of the rear axle $(x_{R,k}, y_{R,k})$, its velocity v_k, yaw angle φ_k and yaw rate ω_k, illustrated in Fig. 1 (blue). The geometric part describes the object's extent. In this case, the shape is approximated by a rectangle, parametrized by its length l_k and width b_k. The complete state vector then is

$$\boldsymbol{\xi}_k = \begin{bmatrix}x_{R,k}, & y_{R,k}, & v_k, & \varphi_k, & \omega_k, & l_k, & b_k\end{bmatrix}^\mathrm{T}. \quad (1)$$

The rectangle is aligned with the orientation φ_k and its position is fixed to $(x_{R,k}, y_{R,k})$, such that b is symmetrically arranged and the length to the front is $0.77l$. This value was determined to be a good approximation for vehicles.

B. Measurement Vector

Measurements obtained at time index k are summarized in the measurement set $Z_k = \{\boldsymbol{z}_k^1, \dots, \boldsymbol{z}_k^j, \dots, \boldsymbol{z}_k^M\}$. The presented model processes raw radar measurements on target level without data preprocessing, feature extraction or clustering. Every measurement contains the radial distance r from measurement to sensor, the angle θ in SCs and the range rate or Doppler velocity v_d (see also Fig. 1 (red)):

$$\boldsymbol{z}_k^j = \begin{bmatrix}r_k^j, & \theta_k^j, & v_{d,k}^j\end{bmatrix}^\mathrm{T}. \quad (2)$$

III. Measurement Model

The measurement model consists of three parts: a target measurement likelihood $p(\boldsymbol{z}|\boldsymbol{\xi})$ of a single target measurement, a clutter likelihood $P_C = p(\boldsymbol{z})$ for clutter measurements and a method to cover different association hypotheses ψ.

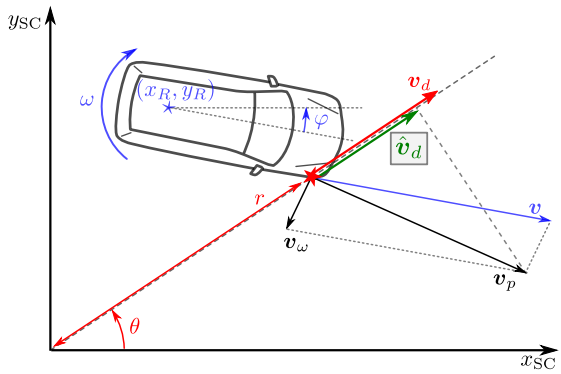

Fig. 1. Derivation of the expected Doppler velocity $\hat{v}_d$

A. Target Measurement Likelihood

Applying the Bayesian chain rule, the target likelihood of a single measurement $\boldsymbol{z}$ is split up in individual components describing the range rate, the radial distance and the angle:

$$p(\boldsymbol{z}|\boldsymbol{\xi}) = p(r, \theta, v_d|\boldsymbol{\xi}) = p(v_d|r, \theta, \boldsymbol{\xi}) \cdot p(r|\theta, \boldsymbol{\xi}) \cdot p(\theta|\boldsymbol{\xi}). \quad (3)$$

The individual components are detailed in the following.

1) Doppler Model $p(v_d|r, \theta, \boldsymbol{\xi})$: The measurement error of the Doppler velocity is assumed to be Gaussian. Therefore, its likelihood is modeled by the normal distribution

$$p(v_d|r, \theta, \boldsymbol{\xi}) = \mathcal{N}(v_d; \hat{v}_d(r, \theta, \boldsymbol{\xi}), \sigma_v^2) \quad (4)$$

with mean $\hat{v}_d$ and variance σ_v^2. The mean value $\hat{v}_d$ corresponds to the expected Doppler velocity at the location (r, θ) of the measurement. Given the object's state and the measurement location, the expected Doppler velocity $\hat{v}_d$ is derived geometrically as shown in Fig. 1. The velocity vector $\boldsymbol{v}_p$ of any point on the object is described through the superposition of the object's velocity $\boldsymbol{v} = v \cdot \begin{bmatrix}\cos\varphi, & \sin\varphi, & 0\end{bmatrix}^\mathrm{T}$ in its direction of motion and the velocity $\boldsymbol{v}_\omega(r, \boldsymbol{\xi}) = \boldsymbol{\omega} \times \boldsymbol{r}_R$ resulting from the object's yaw rate ω:

$$\boldsymbol{v}_p(r, \boldsymbol{\xi}) = \boldsymbol{v} + \boldsymbol{v}_\omega = \begin{bmatrix} v \cdot \cos\varphi - \omega(r \cdot \sin\theta - y_R) \\ v \cdot \sin\varphi + \omega(r \cdot \cos\theta - x_R) \\ 0 \end{bmatrix}. \quad (5)$$

The expected Doppler velocity $\hat{v}_d(r, \theta, \boldsymbol{\xi})$ is the result of the scalar projection of $\boldsymbol{v}_p(\boldsymbol{\xi}, r)$ on the normalized vector $\begin{bmatrix}\cos\theta, & \sin\theta, & 0\end{bmatrix}^\mathrm{T}$, yielding its radial portion:

$$\begin{aligned}\hat{v}_d(\theta, \boldsymbol{\xi}) &= \hat{v}_d(r, \theta, \boldsymbol{\xi}) \\ &= v \cdot \cos(\theta - \varphi) + \omega\left(y_R \cdot \cos\theta - x_R \cdot \sin\theta\right).\end{aligned} \quad (6)$$

Hence, the expected Doppler velocity is independent of the range r and as a consequence $p(v_d|r, \theta, \boldsymbol{\xi}) = p(v_d|\theta, \boldsymbol{\xi})$.

2) Range Model $p(r|\theta, \boldsymbol{\xi})$: To model the range probability, for each measurement, the wave propagation path is approximated by an imaginary ray. Along this ray, a probability density is defined. A Gaussian mixture model is used, as the range measurement error is expected to be Gaussian. At each point of the ray where a measurement

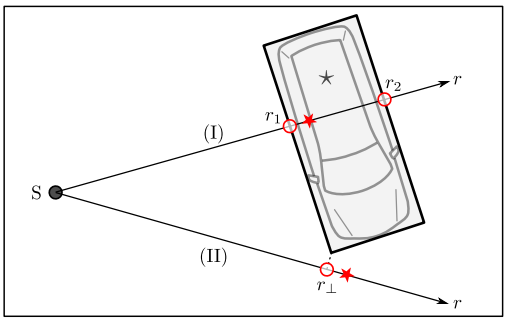

(a) Range model concept based on rays

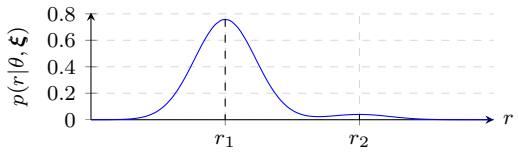

(b) Function profile of the range likelihood in case (I)

Fig. 2. Range model $p(r|\theta,\boldsymbol{\xi})$; In (a) all intersection scenarios (I) and (II) of a ray from sensor S through a measurement (★) are illustrated. A red circle (○) denotes a peak of a Gaussian in the likelihood function. Figure (b) shows the function profile for scenario (I) resulting from (7).

is most likely to arise, a Gaussian is set up. Typically, radar measurements caused by vehicles originate mostly from their contour facing the sensor and less from their interior or averted edges. However, also measurements that are a result of reflections from the road surface to the vehicles underbody or averted edges are possible. Compared to measurements from facing edges, they occur rather infrequently. Besides, in this case, the traveled path of the wave is not equivalent to the actual range and thus error-prone. Based on these observations, two cases and realizations of the range model are to be distinguished, as shown in Fig. 2a.

In case (I), the measurement is located such that the imaginary ray intersects the shape twice. The Gaussian mixture then consists of two mixture components located at the intersection points. This yields the probability density

$$p_{\mathrm{I}}(r|\theta,\boldsymbol{\xi}) = \frac{1}{\sqrt{2\pi\cdot\sigma_r^2}}\cdot\sum_{i=1}^{2} c_i\cdot \mathrm{e}^{-\frac{(r_i-r)^2}{2\cdot\sigma_r^2}}. \tag{7}$$

The mean values r_i are the distances from the sensor to the intersection points. They are a function of the object state $\boldsymbol{\xi}$ since their values depend on the object's position and extent. The coefficients c_i are used to weight the Gaussians and are empirically chosen to be $c_1 = 0.95$ and $c_2 = 0.05$. In Fig. 2b, an exemplary probability density profile of (7) is shown.

In case (II), the measurement is located such that the ray is not intersecting the object's contour. The probability density is approximated by a single Gaussian

$$p_{\mathrm{II}}(r|\theta,\boldsymbol{\xi}) = \frac{1}{\sqrt{2\pi\cdot\sigma_r(r_\perp)^2}}\cdot \mathrm{e}^{-\frac{(r_\perp-r)^2}{2\cdot\sigma_r(r_\perp)^2}} \tag{8}$$

with the expected value at $r_\perp$. It describes the distance between the sensor and the point of the ray closest to any object corner. This point is determined by the orthogonal projection of the corner to the ray (see Fig. 2a). Since the density should converge to the clutter probability with increasing $r_\perp$, the deviation $\sigma_r(r_\perp)$ increases proportionally with $r_\perp$.

3) Angle Model $p(\theta|\boldsymbol{\xi})$: It is assumed, that the probability of receiving a target measurement from the object at a specific angle is uniformly distributed on the angle interval $B(\boldsymbol{\xi}) = [\beta_{\min}, \beta_{\max}]$. The density over the field of view (FOV) angle range is given by

$$p(\theta|\boldsymbol{\xi}) = \begin{cases} \frac{1}{\beta_{\max}-\beta_{\min}}, & \text{if } \theta \in B(\boldsymbol{\xi}) \\ 0, & \text{otherwise} \end{cases}. \tag{9}$$

The angle interval limits $\beta_{\min}$ and $\beta_{\max}$ are chosen such that a density approximately invariant of the object orientation φ is obtained. This is achieved by using the angle range covered by smallest enclosing circle of the object. In this way, the angle ranges for different object orientations are approximately the same.

B. Clutter Model

A radar sensor not only provides measurements originating from the target object but also from other objects in the FOV, such as traffic signs or road marker posts. Additionally, random clutter occurs, for example from the rough road surface. For this reason, a clutter measurement likelihood model is required. Clutter measurements are assumed to be uniformly distributed on the sensor measurement volume $V = \Delta r_{\text{sensor}}\cdot\Delta\theta_{\text{sensor}}\cdot\Delta v_{d,\text{sensor}}$ with probability

$$P_C = p(\boldsymbol{z}) = p(r)\cdot p(\theta)\cdot p(v_d) = \frac{1}{V}. \tag{10}$$

C. Association and Likelihood Formulation

Each measurement in Z is assigned to either target (T) or clutter (C). Since the correct association is unknown, different possibilities ψ must be evaluated. For each association, the product of the measurement likelihood of all measurements in Z is evaluated using

$$p(Z|\boldsymbol{\xi},\psi) = \prod_{\boldsymbol{z}\in C(\psi)} p(\boldsymbol{z})\cdot\prod_{\boldsymbol{z}\in T(\psi)} p(\boldsymbol{z}|\boldsymbol{\xi}). \tag{11}$$

All possible associations ψ are summarized in Ψ, with the number of possible associations $|\Psi|$. Since all associations are assumed equally likely, the combined measurement likelihood of all associations is given by its mean value

$$p(Z|\boldsymbol{\xi}) = \frac{1}{|\Psi|}\cdot\sum_{\psi\in\Psi}\prod_{\boldsymbol{z}\in C(\psi)} p(\boldsymbol{z})\cdot\prod_{\boldsymbol{z}\in T(\psi)} p(\boldsymbol{z}|\boldsymbol{\xi}). \tag{12}$$

IV. Particle Filter Implementation

In this section, the realization of the presented measurement model in a tracking filter is introduced. Due to the highly nonlinear measurement model, a particle filter [14] is applied. The joint posterior probability density function $p(\boldsymbol{\xi}_k|Z_k)$ can be factorized such that

$$p(\boldsymbol{\xi}_k|Z_k) = p(\boldsymbol{x}_k,\boldsymbol{g}_k|Z_k) = p(\boldsymbol{g}_k|\boldsymbol{x}_k,Z_k)\cdot p(\boldsymbol{x}_k|Z_k). \tag{13}$$

By using a Rao-Blackwellized particle filter (RBPF) scheme [14], [15], the kinematic portion $p(\boldsymbol{x}_k|Z_k)$ is estimated using particles, whereas the geometry is represented by a discrete distribution which is updated with a discrete Bayes filter. This allows a simple, approximate, and analytical estimation of the object dimensions and hence, to reduce the amount of required particles in the filter. The discrete density $p(\boldsymbol{g}_k|\boldsymbol{x}_k, Z_{1:k})$ consists of a finite amount of elements that represent specific length-width combinations. At the beginning of each iteration, the density contains a single element which represents the current size hypothesis. The density is then locally expanded by adding new elements close to the current hypothesis, updated using a discrete Bayes filter, and again reduced to a new hypothesis by computing the mean value. Note that the density is discrete in that it only contains a finite and varying amount of elements. The respective values, however, depend on the introduced variation and are not discretized.

A. Prediction

The prediction is divided into two independent parts: a kinematic prediction which uses a constant turn rate and velocity (CTRV) model for $\boldsymbol{x}_k$, and a geometric prediction step which adds the new size hypotheses. The two-dimensional discrete geometry density, consisting of a single element, is expanded through discrete convolution with a symmetric 3×3 equal weights convolution kernel with distances of $\pm\Delta l$ and $\pm\Delta b$ in length and width around the center. As the center of motion is influenced by the object's dimensions, a change of those may cause an erroneous change of the position (x_R, y_R). To circumvent this problem, the extent is modified relative to (x_R, y_R) which is kept fix during geometry prediction.

B. Update

The likelihood of a rectangular object with specific extent l and b is given by the measurement model. The geometry prior is represented by the discrete density $p(\boldsymbol{g}_k|\boldsymbol{x}_k, Z_{1:k-1})$ where $Z_{1:k-1}$ denotes all measurements up to $k-1$. Since the kinematic state is estimated through a particle filter, the kinematic posterior $p(\boldsymbol{x}_k|Z_{1:k})$ is approximated by drawing particles according to its prior $p(\boldsymbol{x}_k|Z_{1:k-1})$, the proposal density. The importance weight is then proportional to

$$w \sim \frac{p(\boldsymbol{x}_k|Z_{1:k})}{p(\boldsymbol{x}_k|Z_{1:k-1})} = p(Z_k|\boldsymbol{x}_k, Z_{1:k-1}). \tag{14}$$

Applying the law of total probability, the unnormalized weight is

$$\begin{aligned} \tilde{w} &= \sum_{\boldsymbol{g}_k} p(Z_k|\boldsymbol{x}_k, \boldsymbol{g}_k) \cdot p(\boldsymbol{g}_k|\boldsymbol{x}_k, Z_{1:k-1}) \\ &= \sum_{\boldsymbol{g}_k} \underbrace{p(Z_k|\boldsymbol{\xi}_k)}_{(12)} \cdot \underbrace{p(\boldsymbol{g}_k|\boldsymbol{x}_k, Z_{1:k-1})}_{\text{geometry prior}}. \end{aligned} \tag{15}$$

C. Implementation Details

The filter is initialized with plausible particles obtained through analysis of a single sensor snapshot. Also, to reduce complexity and computational effort, some simplifications are applied to the filter concerning association hypotheses and the geometry density sample reduction.

1) Association Hypotheses: To reduce the number of association hypotheses of the measurements to clutter (C) or target (T), two simplifications are introduced. First, a geometric rectangular gating is performed such that only measurements within a defined proximity to the object may be assigned to T. All measurements outside this gating area are assigned to C for all hypotheses, reducing the number of association possibilities. Secondly, the M' gated measurements in target proximity are sorted according to their likelihood (3). For $m_T = 0 \dots M'$, the m_T-th association hypothesis assigns the best m_T measurements to T, all others are assigned to C. This results in $M'+1$ different association hypotheses with $M' \leq M$.

2) Geometry Density: The geometry prior consists of N_g uniformly distributed elements with probability $1/N_g$. Then the weight (15) reduces to

$$\tilde{w} = \frac{1}{N_g} \sum_{\nu=1}^{N_g} p(Z_k|\boldsymbol{x}_k, \boldsymbol{g}_k^{[\nu]}). \tag{16}$$

Since a convolution is computed for the geometric density in the prediction step, the number of elements in this density would increase over time. Therefore, the geometric density is reduced to its mean value after the update. To obtain feasible length-width combinations, elements in the density exceeding upper and lower limits for both states as well as a minimum and maximum ratio l/b are discarded.

V. Evaluation

To evaluate the presented filter, real sensor data of various traffic and motion scenarios are used, such as roundabouts, intersections, overtaking maneuvers, or longitudinal traffic. Additionally, a scenario in which a vehicle is driving an eight in front of the sensor is evaluated. The data is recorded with a test vehicle, the ego-vehicle, which is equipped with a 76 GHz high-resolution short range radar covering a FOV of $\pm 75°$ in azimuth and about $45\,\mathrm{m}$ in range. The frame rate of the sensor is $50\,\mathrm{ms}$. Since the used motion scenarios comprise situations with a moving ego-vehicle, ego-motion compensation is required for both the tracks maintained in ego-vehicle coordinates as well as for the measured range rate. To obtain the ego-motion as well as a reliable ground truth of the reference vehicle, both vehicles are equipped with a DGPS and IMU providing accurate measurements of their individual location, orientation and motion.

The focus of this tracking application is to estimate the kinematic states and track other vehicles in traffic to predict their behavior and avoid dangerous situations. In this context, it is important that the estimated extent can be adapted to the given situation through the measurement model. Provided measurement points exist along a sufficiently large portion of either the length or the width of the vehicle, the estimated extent should reflect the visible extent. Furthermore, the location of the object's visible edges must be correct.

The filter results are compared to the known ground truth provided by the DGPS and IMU. Determined beforehand

using simulations, the particle quantity is set to 200 which offers a sufficient robustness and accuracy for most tested scenarios with a track loss of less than 5%. The results presented in the following are obtained through 100 filter runs per scenario and are evaluated focussing on the root mean square error (RMSE). Depending on the situation, the state parameters can be estimated with differing accuracy due to different observability of the parameters. Exemplarily, the results of a single scenario are presented. In this scenario, the reference vehicle drives an eight in front of the ego-vehicle. An extract of the scenario with an exemplary tracking result is given in Fig. 3. The scenario provides a lot of dynamics in all kinematic parameter trajectories and thus requires a lot of flexibility and dynamic from the filter and at the same time covers multiple sensor-to-object alignments.

TABLE I
ROOT MEAN SQUARE ERROR (RMSE) OF THE KINEMATIC STATES

State	x_R[m]	y_R[m]	φ[rad]	v[m/s]	ω[rad/s]
Eight scenario	0.282	0.576	0.114	0.473	0.186
All scenarios	0.394	0.567	0.201	0.663	0.139

In Fig. 4, the trajectories of the different states, the corresponding RMSE and the number of available measurements over time index k are shown. The overall RMSE of the kinematic states for the evaluated test scenario and the mean RMSE for all scenarios, in total ten, is given in Table I.

The estimated trajectories for the center of motion (see Fig. 4a) and yaw angle (see Fig. 4b) are quite similar to their real trajectories and show only small deviations. Due to the sensor-to-object alignment, larger errors in the estimate of the y_R-position occur at the upper and lower curves of the eight (k between 80-100 and 190-220). Even so, this is a good result considering the position of the center of motion is not directly observable. Furthermore, through the measurement model, it is linked directly to the object's extent and thus is affected by its estimate accuracy as well. The estimate of the yaw angle is at an RMSE of approximately $0.114\,\mathrm{rad}$ or $6.5°$ better than the average RMSE. It shows, that this parameter is noticeably correlated to the number of available measurements especially along the vehicle's edges. An increasing number of such measurements usually results in an improved estimate of the yaw angle at subsequent points of time. For example, a distinct increase of the RMSE is observable around $k \approx 280$ where no measurements are available from the object for several points in time.

The velocity and yaw rate exhibit a higher fluctuation than position and yaw angle (see Figs. 4c and 4d). They approximately follow their real trajectory but show more deviation and in some intervals high fluctuations and deflections. For the velocity, temporary RMSEs up to $1.5\,\mathrm{m/s}$ occur at an overall RMSE of about $0.473\,\mathrm{m/s}$ or $1.7\,\mathrm{km/h}$. For the estimate of the yaw rate, some larger deflections are observable as well. However, considering the high dynamics and values of the yaw rate of more than $\pm 1\,\mathrm{rad/s}$, a peak RMSE of $0.5\,\mathrm{rad/s}$ at an overall RMSE of $0.186\,\mathrm{rad/s}$ or $10.66\,°/\mathrm{s}$ is adequate.

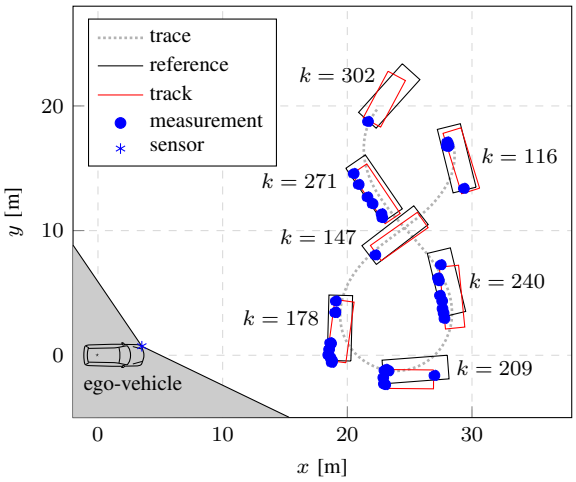

Fig. 3. Extract of the eight scenario from $k = 116$ to 302

The results of the estimated extent depend on the observability of the particular parameter and the distribution of the measurements along it. If measurements along a complete edge are visible due to the sensor-to-object alignment, for example the length at $k = 178$ and $k = 271$ in Fig. 3, the estimate is approximately the actual length. This is also observable in Fig. 4f for k from 240 to 270. The large RMSE at the beginning of the sequence up to $k = 100$ results from the orientation of the vehicle. Since it approaches the sensor head on, the total length is not observable. Whereas the estimate of the completely visible width shows good results for the same time interval (see Fig. 4e). A total RMSE of $0.323\,\mathrm{m}$ in width and $0.832\,\mathrm{m}$ in length is achievable, even though temporarily the length or width is not visible to the sensor. The average RMSE is slightly better in width with $0.252\,\mathrm{m}$ and a bit larger in length with $1.019\,\mathrm{m}$. Since many of the used scenarios represent real traffic scenarios with driving behind or in front of the observed vehicle, it is reasonable that the mean estimate in width is better than in length.

VI. CONCLUSION

This paper introduced a new vehicle measurement model for high-resolution radars based on direct scattering. The measured range, angle and Doppler velocity can be exploited in arbitrary sensor-to-object alignments to estimate the kinematic state of a vehicle based on measurements of a single high-resolution radar. Simultaneously, the extent of the object can be estimated. The model was employed and validated in a single-object application using an RBPF and real sensor data. As an extension, the applicability of the measurement model to multi-sensor and multi-object scenarios has been studied in the associated publication [16].

ACKNOWLEDGMENT

This work was partly supported by the German Research Foundation (DFG) within the Transregional Collaborative Research Center SFB/TRR 62 Companion-Technology for Cognitive Technical Systems.

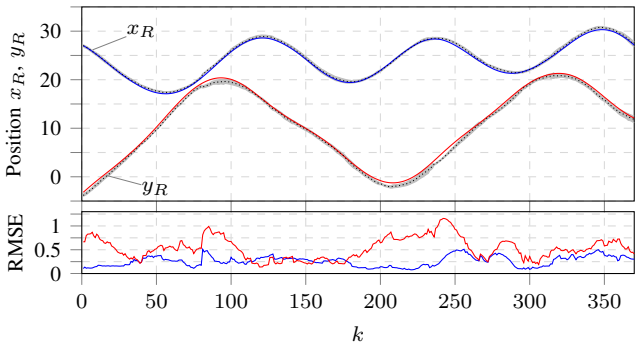

(a) Position x_R, y_R and RMSE in m

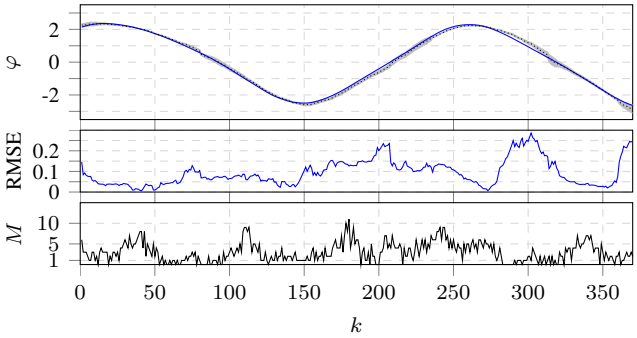

(b) Yaw angle φ and RMSE in rad

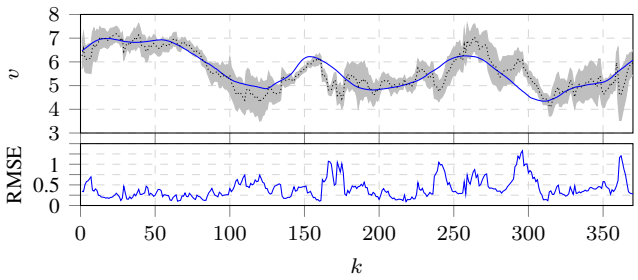

(c) Velocity v and RMSE in m/s

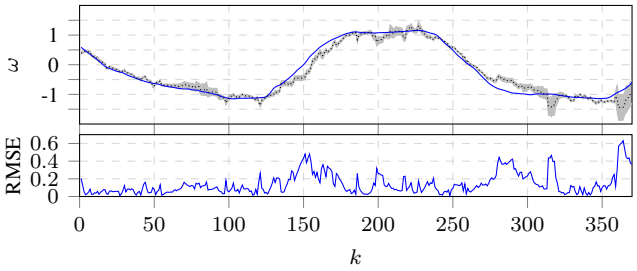

(d) Yaw rate ω and RMSE in rad/s

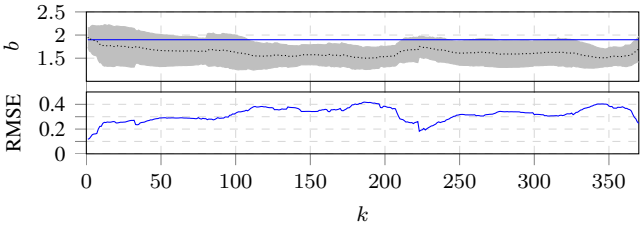

(e) Width b and RMSE in m

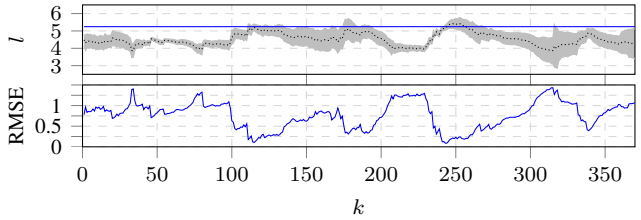

(f) Length l and RMSE in m

Fig. 4. Evaluation results of the 8-trajectory for the different states; The upper graphs show the true trajectories (solid) and the mean estimates (dotted) of the different states over time k. The gray area represents the 2σ deviation of the estimate. In the lower graphs, the corresponding RMSE is plotted. In Figure (b), the number M of available measurements is given in the additional graph.

References

[1] D. Kellner and J. Klappstein, "Instantaneous Lateral Velocity Estimation of a Vehicle using Doppler Radar," *16th International Conference on Information Fusion (FUSION)*, pp. 877–884, 2013.

[2] D. Kellner, M. Barjenbruch, J. Klappstein, J. Dickmann, and K. Dietmayer, "Instantaneous Full-Motion Estimation of Arbitrary Objects using Dual Doppler Radar," in *IEEE Intelligent Vehicles Symposium, Proceedings*, 2014, pp. 324–329.

[3] M. Buhren and B. Yang, "Simulation of Automotive Radar Target Lists using a Novel Approach of Object Representation," *IEEE Intelligent Vehicles Symposium*, pp. 314–319, 2006.

[4] J. Gunnarsson, L. Svensson, L. Danielsson, and F. Bengtsson, "Tracking vehicles using radar detections," *IEEE Intelligent Vehicles Symposium, Proceedings*, pp. 296–302, 2007.

[5] L. Hammarstrand, L. Svensson, F. Sandblom, and J. Sörstedt, "Extended Object Rracking using a Radar Resolution Model," *IEEE Transactions on Aerospace and Electronic Systems*, vol. 48, no. 3, pp. 2371–2386, 2012.

[6] K. Gilholm and D. Salmond, "Spatial distribution model for tracking extended objects," *IEE Proceedings - Radar, Sonar and Navigation*, vol. 152, no. 5, pp. 364–371, 2005.

[7] K. Gilholm, S. Godsill, S. Maskell, and D. Salmond, "Poisson models for extended target and group tracking," in *SPIE Conference: Signal and Data Processing of Small Targets*, 2005.

[8] M. Baum, B. Noack, and U. D. Hanebeck, "Extended Object and Group Tracking with Elliptic Random Hypersurface Models," in *13th Conference on Information Fusion (FUSION), Proceedings*, 2010.

[9] M. Baum and U. D. Hanebeck, "Shape Tracking of Extended Objects and Group Targets with Star-Convex RHMs," in *14th International Conference on Information Fusion (FUSION), Proceedings of the*, 2011.

[10] W. Koch, "Bayesian Approach to Extended Object and Cluster Tracking using Random Matrices," *IEEE Transactions on Aerospace and Electronic Systems*, vol. 44, no. 3, pp. 1042–1059, 2008.

[11] M. Feldmann, D. Fränken, and W. Koch, "Tracking of Extended Objects and Group Targets Using Random Matrices," *IEEE Transactions on Signal Processing*, vol. 59, no. 4, pp. 1409–1420, 2011.

[12] M. Feldmann and D. Fränken, "Advances on Tracking of Extended Objects and Group Target Using Random Matrices," in *12th International Conference on Information Fusion (FUSION), Proceedings*, no. 1, 2009, pp. 1029–1036.

[13] A. Petrovskaya and S. Thrun, "Model Based Vehicle Detection and Tracking for Autonomous Urban Driving," *Autonomous Robots*, vol. 26, pp. 123–139, apr 2009.

[14] B. Ristic, S. Arulampalam, and N. Gordon, *Beyond the Kalman Filter: Particle Filters for Tracking Applications*. Artech House, 2004.

[15] "Rao-Blackwellized Particle Filtering for Dynamic Bayesian Networks," in *Sequential Monte Carlo Methods in Practice*, A. Doucet, N. de Freitas, and N. Gordon, Eds. Springer New York, 2001, pp. 499–515.

[16] A. Scheel, C. Knill, S. Reuter, and K. Dietmayer, "Multi-Sensor Multi-Object Tracking of Vehicles Using High-Resolution Radars," in *IEEE Intelligent Vehicles Symposium*, 2016.